Asynchronism and nonequilibrium phase transitions in $(1+1)$D quantum cellular automata

Edward Gillman,[1,2] Federico Carollo,[3] and Igor Lesanovsky[1,2,3]

[1] *School of Physics and Astronomy, University of Nottingham, Nottingham, NG7 2RD, UK*
[2] *Centre for the Mathematics and Theoretical Physics of Quantum Non-Equilibrium Systems, University of Nottingham, Nottingham, NG7 2RD, UK*
[3] *Institut für Theoretische Physik, Universität Tübingen, Auf der Morgenstelle 14, 72076 Tübingen, Germany*

Probabilistic cellular automata provide a simple framework for exploring classical nonequilibrium processes. Recently, quantum cellular automata have been proposed that rely on the propagation of a one-dimensional quantum state along a fictitious discrete time dimension via the sequential application of quantum gates. The resulting $(1+1)$-dimensional space-time structure makes these automata special cases of recurrent quantum neural networks which can implement broad classes of classical nonequilibrium processes. Here, we present a general prescription by which these models can be extended into genuinely quantum non-equilibrium models via the systematic inclusion of *asynchronism*. This is illustrated for the classical contact process, where the resulting model is closely linked to the quantum contact process (QCP), developed in the framework of open quantum systems. Studying the mean-field behaviour of the model, we find evidence of an "asynchronism transition", i.e. a sudden qualitative change in the phase transition behavior once a certain degree of asynchronicity is surpassed, a phenomenom we link to observations in the QCP.

Nonequilibrium processes can display collective effects and critical behavior. In the vicinity of nonequilibrium phase transitions (NEPTs), the resulting phenomenology can show macroscopic features that are shared by different models. This so-called universality allows for diverse systems to be gathered into few classes, enabling the investigation of emergent phenomena through the analysis of minimal models within a class [1, 2]. For classical systems, a paradigmatic setting for exploring nonequilibrium universality is that of $(1+1)$D cellular automata (CA). These consist of 2D models realising an effective 1D system discrete-time dynamics, as shown in Fig. 1(a). The propagation of the 1D state from time t to $t+1$ occurs through the sequential application of local gates (or rules) operating on the (target) row $t+1$, controlled by the state of row t, see Fig. 1(a). Such classical dynamics can either be deterministic, usually implemented through unitary gates, or probabilistic, with non-unitary local updates. In the latter case, by suitably choosing the gates, these automata provide discrete-time versions of continuous-time dynamics [1]. Owing to their simple structure, this has allowed for a deep understanding of several classical nonequilibrium processes [1–7].

Recently, quantum versions of these automata have been introduced and dubbed $(1+1)$D quantum cellular automata (QCA) [8–10]. These models are particularly appealing for at least two reasons. Firstly, they can be realized on current quantum simulators [11–14]. Secondly, while closely linked to unitary 1D QCA [15–19], $(1+1)$D QCA are equivalent to quantum neural networks (QNNs) applied in quantum machine learning (QML) [20]. In the language of QNNs, the first and last rows of the QCA correspond to input and output layers respectively, while the intermediate rows are the hidden layers [cf. Fig. 1(a)]. The local gate of the QCA is then a N-input, one-output quantum perceptron, and a quantum evolution proceeds by applying the gate layer by layer, just as in QNNs. Since every perceptron is identical, QCA are in fact recurrent QNNs. With regards to the study of nonequilibrium processes, $(1+1)$D QCA are also particularly effective as they include their classical counterparts as a limiting case, requiring only *synchronous* updates –i.e. commuting gates. For instance, probabilistic cellular automata (PCA) can be reproduced through commuting unitary quantum gates. The QCA state displays non-classical properties [8, 21], but nonetheless captures the classical model, with diagonal elements coinciding with the probabilities of the associated PCA.

In this paper, we present a prescription for extending a given classical model into a genuinely quantum model via the systematic inclusion of *asynchronism* in the $(1+1)$D QCA framework [cf. Fig. 1(b)]. Asynchronism alone is not necessarily a quantum feature [22–24]. However, in QCA, asynchronous — non-commuting — gates can generate a dependence between diagonal observables of one time slice and coherence in the previous one [Fig. 1(c)]. After presenting the general prescription, we analyze the case of the classical *contact process* (CCP). Remarkably, we find that the QCA resulting from the introduction of asynchronism is closely connected to the continuous-time *quantum contact process* (QCP) [25–30]. To make the link precise, we compare the mean-field equations of the QCP and of the asynchronous QCA. We find that the quantum Hamiltonian contribution in the QCP is analogous to the one due to asynchronism in the QCA. We further investigate the QCA mean-field phase diagram. While for low asynchronism it displays a second-order NEPT in the directed percolation (DP) universality class,

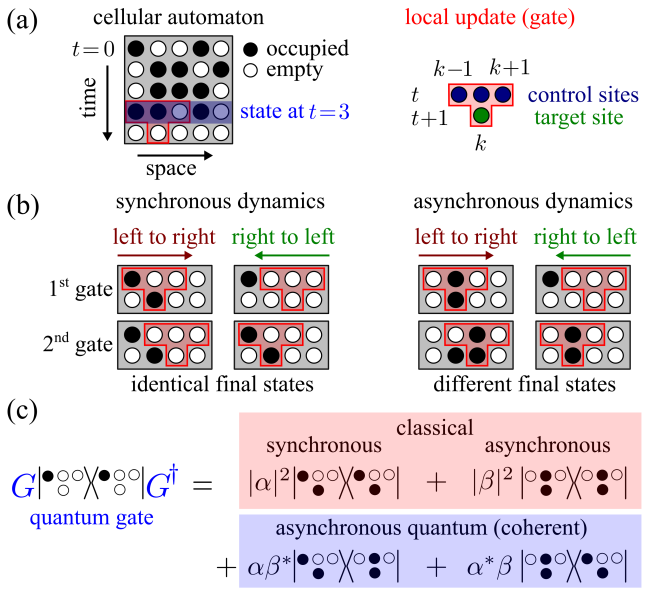

FIG. 1. **Asynchronism in classical CA and $(1+1)$D QCA:** (a) A CA consists of a 2D lattice of two-level systems, which can either be in an occupied or empty state. The vertical dimension of the lattice provides an effective discrete-time dimension and propagation along the time direction is achieved through the sequential application of local gates. These perform operations on a target site at row $t+1$ and in position k according to the state of three control sites (at position $k-1, k, k+1$) in the previous row. After the row $t+1$ has been completely updated, its state represents the state of an effective 1D system at time $t+1$. **(b)** During a single time update, if the local gates do not modify the control sites, the order of their application is irrelevant (synchronous dynamics). If local gates change the control sites, the order of their application is relevant and can produce different final states (asynchronous dynamics). **(c)** While in a classical CA, the occupation of a target site solely depends on occupation probabilities of control sites, asynchronism in a QCA is linked to quantum coherent processes. In the panel, it is shown how an asynchronous gate can generate, in addition to classical asynchronous terms, a coupling between the occupation in the target site and coherence in the control sites.

as expected from the corresponding PCA [3], there exists a critical value of asynchronism above which the NEPT qualitatively changes and becomes first-order. We thus term this an "asynchronism transition". We compare this with the phase diagram estimated using tensor-network techniques, and with similar behavior in the QCP.

Our results present a framework to study the role of quantum effects in nonequilibrium collective behavior. Given that non-commuting gates are required for universal computation on QNNs [20], our work hints at further interesting links between asynchronism, quantum many-body dynamics and quantum machine learning.

Synchronous $(1+1)$D QCA. In the 2D lattice of the QCA, sites can be in the empty $|\circ\rangle$ or occupied $|\bullet\rangle$ state, see Fig. 1(a). The lattice initial state, $|\psi_0\rangle$, is chosen as a product state, where row $t=0$ contains the initial 1D configuration, while the other sites are initialized in $|\circ\rangle$. The 2D lattice evolves iteratively as $|\psi_{t+1}\rangle = \mathcal{G}_t\,|\psi_t\rangle$, where $\mathcal{G}_t$ acts on rows t and $t+1$. This global update is made of the product of local gates $G_{t,k}$, updating the target site at $(t+1,k)$. For example, a given ordering could be $\mathcal{G}_t = \ldots G_{t,k}\ldots G_{t,2}G_{t,1}$. The time-evolved 1D system state is $\rho_t = \mathrm{Tr}'\left(|\psi_t\rangle\langle\psi_t|\right)$, with the trace taken over all sites except those in row t [cf. Fig.1(a)]. See Refs. [9, 10, 21] for further details on $(1+1)D$ QCA.

The simplest local unitary gate is of the form

$$G_{t,k} = \sum_{\mathcal{N}} P_{\mathcal{N}} \otimes U_{\mathcal{N}}\ . \tag{1}$$

Here, $\mathcal{N}$ labels the basis states of the "control" sites in the neighbourhood of site k on row t. For example, a three-site neighbourhood has 8 basis states, $\mathcal{N} = (\circ\circ\circ, \circ\circ\bullet, \ldots, \bullet\bullet\bullet)$. The unitary operator $U_{\mathcal{N}}$ "rotates" the target (on row $t+1$ and in position k) conditioned on the state of the control sites. This is enforced by the projector $P_{\mathcal{N}} = |\mathcal{N}\rangle\langle\mathcal{N}|$ acting on them. We will use the symbol $\otimes$ to separate control sites (to the left) and target sites (to the right). Since in Eq. (1) only orthogonal projectors act on control sites, gates $G_{t,k}$ acting on different target sites commute and the dynamics is synchronous, i.e., target sites can be updated simultaneously [see Fig. 1(b)].

To illustrate that such synchronous $(1+1)$D QCA allows for the implementation of a range of canonical nonequilibrium models [4, 5, 31, 32] we consider the realization of the so-called contact process [3, 6]. The contact process features three elementary ingredients: decay, i.e. the transition of a site from occupied to empty ($\bullet \rightsquigarrow \circ$); coagulation, which is also the transition of a site from full to empty but facilitated (conditioned) by one of its neighbors ($\bullet\bullet \rightsquigarrow \bullet\circ$); and branching, which is facilitated excitation of the form $\bullet\circ \rightsquigarrow \bullet\bullet$. Note that the contact process possesses the absorbing state $\ldots\circ\circ\circ\ldots$ from which no escape is possible. Whether this state is reached at stationarity depends on the rates (or probabilities) of the elementary processes. An instance of the contact process on a (1+1)D QCA is realized by the gate

$$\begin{aligned} G_{t,k} = {} & \Pi_k n_k \otimes U_{\circ\bullet\circ} + \Pi_k \overline{n}_k \otimes \mathbb{1} \\ & + \bar{\Pi}_k n_k \otimes U_{\bullet} + \bar{\Pi}_k \overline{n}_k \otimes U_{\circ}, \end{aligned} \tag{2}$$

which has the form of Eq. (1). Here $n_k = |\bullet\rangle\langle\bullet|_k$ and $\overline{n}_k = |\circ\rangle\langle\circ|_k = \mathbb{1} - n_k$ project onto the occupied and empty state of site k, respectively. Furthermore, we have defined the projectors $\Pi_k = \overline{n}_{k-1}\overline{n}_{k+1}$ and their complements $\bar{\Pi}_k = \mathbb{1} - \Pi_k$. The unitaries U_α, with labels $\alpha = (\circ\bullet\circ, \bullet, \circ)$, perform a (coherent) flip of the target site, which is conditioned on the state of the controls. Note that the first unitary considers the case of empty left/right control sites, while the latter two unitaries act on the target only if at least one of the left/right control sites is occupied. They are parametrized as $U_{\circ\bullet\circ} =$

$\sqrt{p_{\circ\bullet\circ}}\,\mathbb{1}-i\sqrt{q_{\circ\bullet\circ}}\,\sigma^x$ and $U_{\circ/\bullet}=\sqrt{q_{\circ/\bullet}}\,\mathbb{1}-i\sqrt{p_{\circ/\bullet}}\,\sigma^x$ with $\sigma^x=|\bullet\rangle\langle\circ|+|\circ\rangle\langle\bullet|$. The parameters $q_{\circ\bullet\circ}$ and $p_{\circ/\bullet}\in[0,1]$ are the flipping probabilities, and $q_\alpha=1-p_\alpha$.

In the gate in Eq. (2), the control sites have been separated by singling out the central one, so that we can associate to the target site [in position $(t+1,k)$] a specific control site [the one in position (t,k)], which we regard as its "past". This allows for the mean occupation number, $\langle n_k\rangle_{t+1}$, of the target to be calculated iteratively as,

$$\begin{aligned}\langle n_k\rangle_{t+1}&=q_{\circ\bullet\circ}\langle\Pi_k n_k\rangle_t+p_\bullet\langle\bar\Pi_k n_k\rangle_t+p_\circ\langle\bar\Pi_k\bar n_k\rangle_t \qquad (3)\\ &\approx q_{\circ\bullet\circ}\langle\Pi_k\rangle_t\langle n_k\rangle_t+p_\bullet\langle\bar\Pi_k\rangle_t\langle n_k\rangle_t+p_\circ\langle\bar\Pi_k\rangle_t\langle\bar n_k\rangle_t,\end{aligned}$$

where we performed a mean-field decoupling in the second line [33]. This form makes the interpretation of the probabilities entering the unitaries U_α rather transparent: $q_{\circ\bullet\circ}$ is the probability that the target site k gets occupied given that the control site k is occupied while its neighbors are empty. Since the occupation number can only decrease under this process this effectively implements $\bullet\rightsquigarrow\circ$. The probability $p_\bullet$ is the probability of having an occupied target when there is at least one of the external controls and the central one occupied. This also describes a decay process, but here in combination with the so-called *coagulation process*, i.e. the annihilation of two adjacent occupied sites, e.g. $\bullet\bullet\rightsquigarrow\bullet\circ$. Finally, the probability $p_\circ$ parametrizes the strength of a *branching process* ($\bullet\circ\rightsquigarrow\bullet\bullet$). All these ingredients yield the contact process [6]. Finally, by taking the continuous-time limit of Eq. (3), i.e. expanding $\langle n_k\rangle_{t+1}\approx\langle n_k\rangle_t+\Delta t\frac{d}{dt}\langle n_k\rangle_t$, with small time step Δt, one obtains a continuous-time contact process [6] with coagulation rate $\kappa_{\rm c}=(q_{\circ\bullet\circ}-p_\bullet)/\Delta t$, branching rate $\kappa_{\rm b}=p_\circ/\Delta t$ and decay rate $\gamma=p_{\circ\bullet\circ}/\Delta t$ [33].

Asynchronous $(1+1)$D QCA. The dynamics in Eq. (3) is classical as it only connects diagonal observables. A natural question is: what is a minimal modification to the gate $G_{t,k}$ which makes diagonal observables at time $t+1$ depend on coherence at the previous time? We achieve this through asynchronism [cf. Fig. 1(b-c)].

To break the commutativity of the gates, we consider terms modifying control sites along with the target one, see Fig. 1(b), via the gates,

$$G_{t,k}=\sum_{\mathcal N}P_{\mathcal N}\otimes U_{\mathcal N}+\sum_{\mathcal N\neq\mathcal N'}|\mathcal N\rangle\langle\mathcal N'|\otimes O_{\mathcal N,\mathcal N'}\ , \qquad (4)$$

where unitarity of $G_{t,k}$ constrains the operators $O_{\mathcal N,\mathcal N'}$. The minimal modification beyond Eq. (1) affects a single control site, i.e. $|\mathcal N\rangle\langle\mathcal N'|=|\mathcal N\rangle\langle\mathcal N|\,\sigma_k^\pm$, where $\sigma^+=|\bullet\rangle\langle\circ|$ and $\sigma^-=|\circ\rangle\langle\bullet|$, such that,

$$G_{t,k}=\sum_{\mathcal N}P_{\mathcal N}\otimes U_{\mathcal N}+\sum_{\mathcal N,\pm}P_{\mathcal N}\sigma_c^\pm\otimes O_{\mathcal N,\pm}. \qquad (5)$$

Here $\sigma_c^\pm$ acts on a chosen site, labelled c. This equation constitutes a prescription for extending any classical model into a quantum one by choosing the operators $O_{\mathcal N,\pm}$, subject to the constraints of unitarity and any desired physics of the original model. In fact, these requirements can be very restrictive, producing an essentially unique mapping from a classical to a quantum system.

As an example, we consider the CCP in Eq. (2). In this case, the additional constraints are the presence of the absorbing state and that the update depends only on whether there are any particles present, but not on their quantity or position. Applying the prescription gives

$$\begin{aligned}G_{t,k}=&\,\Pi_k n_k\otimes U_{\circ\bullet\circ}+\Pi_k\bar n_k\otimes\mathbb{1}\\ &+\sqrt{1-\lambda}\,\left[\bar\Pi_k n_k\otimes U_\bullet+\bar\Pi_k\bar n_k\otimes U_\circ\right]\\ &+\sqrt{\lambda}\,\bar\Pi_k\left[\sigma_k^+\otimes U_\bullet U_+-\sigma_k^-\otimes U_\circ U_+^\dagger\right]\ . \qquad (6)\end{aligned}$$

This gate contains just one additional unitary beyond the synchronous model, $U_+=i\sqrt{q}\,\mathbb{1}-\sqrt{p}\,\sigma^x$, and features two additional parameters, p and λ, with $\lambda\in[0,1]$ controlling the strength of the asynchronism. When $\lambda=0$ we recover Eq. (2). As λ is increased, gates acting on adjacent target sites do not commute, with the norm of the commutator increasing with λ. Considering the analogue of Eq. (3) for the gate in Eq. (6), we find after a mean-field decoupling [33],

$$\begin{aligned}\langle n\rangle_{t+1}=&\,r_{\circ\bullet\circ}\langle\Pi_k\rangle_t\langle n_k\rangle_t+r_\bullet\langle\bar\Pi_k\rangle_t\langle n_k\rangle_t+r_\circ\langle\bar\Pi_k\rangle_t\langle\bar n_k\rangle_t\\ &+r_*\langle\bar\Pi_k\rangle_t\langle\sigma_k^y\rangle_t\,, \qquad (7)\end{aligned}$$

with $\sigma^y=-i\,|\bullet\rangle\langle\circ|+i\,|\circ\rangle\langle\bullet|$. The coefficients are

$$\begin{aligned}r_{\circ\bullet\circ}&=q_{\circ\bullet\circ},\\ r_\bullet&=(1-\lambda)p_\bullet+\lambda\left(\sqrt{p_\circ}\sqrt{q}+\sqrt{p}\sqrt{q_\circ}\right)^2,\\ r_\circ&=(1-\lambda)p_\circ+\lambda(\sqrt{p_\bullet}\sqrt{q}-\sqrt{p}\sqrt{q_\bullet})^2,\\ r_*&=\sqrt{\lambda}\sqrt{1-\lambda}[\sqrt{q}\,(p_\bullet+p_\circ)\\ &\qquad+\sqrt{p}\,(\sqrt{p_\circ}\sqrt{q_\circ}-\sqrt{p_\bullet}\sqrt{q_\bullet})]. \qquad (8)\end{aligned}$$

Crucially, we see that this equation connects the density operator n of the target site with the coherence observable σ^y for the central control, which, as mentioned before, we interpret as the "past" of the target. Only when $r_*=0$, the equation closes on diagonal observables.

Asynchronism transition. To assess the impact of asynchronism on our $(1+1)$D QCA, we investigate the mean-field stationary state [33]. For the following analysis we fix $q_{\circ\bullet\circ}=p_\bullet=p=0.1$. As shown in Fig. 2(a), for any given value of λ the QCA displays an NEPT from the absorbing state with all empty sites to a state with a finite density of occupied sites, $\langle n\rangle_\infty\neq0$. The critical curve separating those two phases can be parametrized by the strength of asynchronism, $\lambda=\lambda_{\rm c}(p_\circ)$. For $\lambda=0$ (not shown) the QCA represents a discrete-time contact process and thus shares with it a continuous phase transition in the DP universality class. This continuous transition persists when increasing λ. However, beyond $\lambda^*\approx0.92$ the phase transition becomes of first-order.

Since this change in the nonequilibrium physics occurs for increasing λ along the critical curve $\lambda_{\rm c}$, we call this

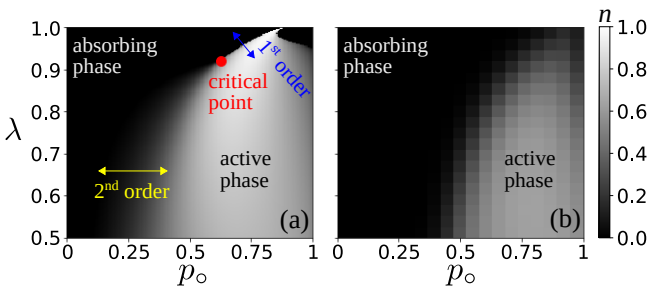

FIG. 2. **Nonequilbrium phase transition in** $(1+1)$**D QCA:** (a) Stationary phase diagram for the model described by the gate (6). An absorbing state phase transition is displayed as a function of the asynchronism parameter λ and the branching probability $p_\circ$. The stationary density is estimated by performing 1000 iterations of the mean-field equations [33]. For strong asychronicity, i.e. $\lambda \gtrsim 0.92$, the phase transition changes from continuous (in the directed percolation universality) to discontinuous. (b) Phase diagram obtained for a $(1+1)$D QCA using tensor networks [21]. Here, the density is calculated using bond-dimension $\chi = 64$, lattice size $L = 64$, and by iterating over 100 time steps.

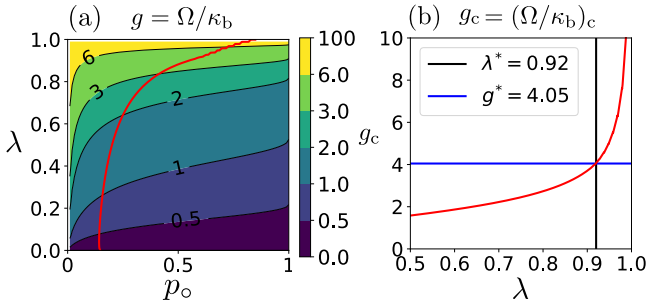

FIG. 3. **Quantum and classical processes in asynchronous** $(1+1)$**D QCA:** (a) By equating Eqs. (8) and (9), the relative strength of quantum to classical branching, $g = \Omega/\kappa_b$, can be examined for the gate in Eq. (6). As can be seen, g (shown as lines of constant value, with coloured areas indicating regions between these values) increases monotonically with the strength of asynchronism in the QCA, parametrised by λ. The solid red line indicates the critical curve of the QCA, estimated by taking the line of constant $n = 0.1$ in the mean-field phase diagram of Fig. 2(a). (b) The behaviour of g along the critical line, denoted as g_c here, is shown for $\lambda \in [0.5, 1]$, and displays a rapid increase with λ. The critical point of the asynchronism transition, λ^*, can be identified with a critical value of $g^* = 4.05$.

an "asynchronism transition". This mean-field transition is expected to be strictly observable above the upper-critical dimension of the model. Instead, to study the $(1+1)$D QCA, we resort to tensor network methods [21], see Fig. 2(b). Here, qualitative agreement with the mean-field solution is found, although the NEPT appears to be continuous throughout. Nevertheless, the emergence of the mean-field phase transition may be signalling a changing universality class in the $(1+1)$D QCA [33]. As we discuss below, this is analogous to the QCP [28–30], which displays a similar phenomenology.

Relation to the quantum contact process. The QCP is a continuous-time Markovian open quantum system that features the same processes as the CCP, with an additional coherent term know as "quantum branching" ($\bullet\circ \leftrightarrow \bullet\bullet$) with rate Ω [25, 26]. This process is implemented by a quantum Hamiltonian, which describes constrained (Rabi) oscillations: sites can only change state when at least one neighbor is occupied. The QCP, as defined in Refs. [25, 26], displays a phase transition from an absorbing state to an active phase. At the mean-field level one finds a change of universal behavior from DP to a first-order transition at a certain critical ratio g^* of quantum and classical branching rates, $g = \Omega/\kappa_b$ [25–27]. In 1D, numerical simulations show that the phase transition in fact remains of second-order throughout. However, there is still a critical value of g above which one finds deviations from DP universality [28–30]. Thus, the QCP displays a change in its universal physics, which at least at a qualitative level is indicated by mean-field.

The close resemblance between the phenomenology of the QCA (6) and the QCP, suggests that the inclusion of asynchronism in the QCA introduces a microscopic process akin to quantum branching [21, 25–30, 34–36]. To verify this, we consider the Heisenberg equation for n of the QCP [25, 26, 33]. Upon discretization with time-step Δt, this is indeed equivalent to Eq. (7) with coefficients,

$$r_{\circ\bullet\circ} = 1 - \gamma\Delta t\ , \qquad r_\bullet = 1 - \gamma\Delta t - \kappa_c\Delta t\ ,$$
$$r_\circ = \kappa_b\Delta t\ , \qquad r_* = \Omega\Delta t\ . \tag{9}$$

Comparing Eq. (9) with Eq. (8), we see that removing asynchronism ($\lambda \to 0$) is equivalent to removing coherent branching ($\Omega\Delta t \to 0$) in the QCP.

Finally, we link the asynchronism transition observed previously with similar behaviour in the QCP, by re-characterising it in terms of the processes of the QCP. Equating Eqs. (9) and (8), we define the parameter $g = \Omega/\kappa_b$ for our QCA, see Fig. 3(a). Clearly, increasing the value of λ corresponds to increasing g. The critical curve, $\lambda = \lambda_c(p_\circ)$, can then also be parametrised by values of g, see Fig. 3(b). In terms of g, the critical point of the asynchronism transition, λ^*, is the point g^*, where quantum branching is sufficiently stronger than classical branching, leading to a change of universal physics in the mean-field phase diagrams and, for $1D$ QCP, in the (non-perturbative) universality class also.

Conclusion. Building on the connection between classical probabilistic CA and continuous-time nonequilibrium dynamics [3, 6], we have demonstrated how asynchronism can be leveraged to gradually introduce genuine quantum effects to an otherwise classical contact process dynamics, and can lead to quantum models that are closely related to those studied in other frameworks. Due to the connection between QCA and QNNs, this analysis might find

application in quantum machine learning, for instance, in providing physical insights into the dynamics of information retrieval and the impact of quantum effects — e.g. caused by asynchronism — on their capability of performing computational tasks.

Acknowledgments. We acknowledge support from EPSRC [Grant No. EP/R04421X/1], from the "Wissenschaftler Rückkehrprogramm GSO/CZS" of the Carl-Zeiss-Stiftung and the German Scholars Organization e.V., as well as through The Leverhulme Trust [Grant No. RPG-2018-181], and the Deutsche Forschungsgemeinschaft through SPP 1929 (GiRyd), Grant No. 428276754, as well as through Grant No. 435696605. We are grateful for access to the University of Nottingham's Augusta HPC service.

[1] M. Henkel, H. Hinrichsen, and S. Lübeck, *Non-Equilibrium Phase Transitions* (Springer Netherlands, 2008).
[2] M. Henkel and M. Pleimling, *Non-Equilibrium Phase Transitions* (Springer Netherlands, 2010).
[3] E. Domany and W. Kinzel, Phys. Rev. Lett. **53**, 311 (1984).
[4] F. Bagnoli, N. Boccara, and R. Rechtman, Phys. Rev. E **63**, 046116 (2001).
[5] F. Bagnoli and R. Rechtman, arXiv preprint (2014), arXiv:1409.4284.
[6] H. Hinrichsen, Adv. Phys. **49**, 815 (2000).
[7] S. Lübeck, Int. J. Mod. Phys. B **18**, 3977 (2004).
[8] I. Lesanovsky, K. Macieszczak, and J. P. Garrahan, Quantum Sci. Technol. **4**, 02LT02 (2019).
[9] E. Gillman, F. Carollo, and I. Lesanovsky, Phys. Rev. Lett. **125**, 100403 (2020).
[10] E. Gillman, F. Carollo, and I. Lesanovsky, Phys. Rev. A **103**, L040201 (2021).
[11] J. Zeiher, R. Van Bijnen, P. Schauß, S. Hild, J.-y. Choi, T. Pohl, I. Bloch, and C. Gross, Nat, Phys. **12**, 1095 (2016).
[12] H. Kim, Y. Park, K. Kim, H.-S. Sim, and J. Ahn, Phys. Rev. Lett. **120**, 180502 (2018).
[13] A. Browaeys and T. Lahaye, Nat. Phys. **16**, 132 (2020).
[14] S. Ebadi, T. T. Wang, H. Levine, A. Keesling, G. Semeghini, A. Omran, D. Bluvstein, R. Samajdar, H. Pichler, W. W. Ho, *et al.*, arXiv:2012.12281 (2020).
[15] K. Wiesner, "Quantum cellular automata," in *Encyclopedia of Complexity and Systems Science*, edited by R. A. Meyers (Springer New York, New York, NY, 2009) pp. 7154–7164.
[16] J. I. Cirac, D. Perez-Garcia, N. Schuch, and F. Verstraete, J. Stat. Mech.-Theory E. **2017**, 083105 (2017).
[17] P. Arrighi, Nat. Comput. **18**, 885 (2019).
[18] T. Farrelly, Quantum **4**, 368 (2020).
[19] L. E. Hillberry, M. T. Jones, D. L. Vargas, P. Rall, N. Y. Halpern, N. Bao, S. Notarnicola, S. Montangero, and L. D. Carr, Quantum Sci. Technol. **6**, 045017 (2021).
[20] K. Beer, D. Bondarenko, T. Farrelly, T. J. Osborne, R. Salzmann, D. Scheiermann, and R. Wolf, Nat. Commun. **11**, 808 (2020).
[21] E. Gillman, F. Carollo, and I. Lesanovsky, Phys. Rev. Lett. **127**, 230502 (2021).
[22] O. Bouré, N. Fatès, and V. Chevrier, Nat. Comput. **11**, 553 (2012).
[23] S. Bandini, A. Bonomi, and G. Vizzari, Nat. Comput. **11**, 277 (2012).
[24] N. Fatès, in *Cellular Automata and Discrete Complex Systems*, edited by J. Kari, M. Kutrib, and A. Malcher (Springer Berlin Heidelberg, Berlin, Heidelberg, 2013) pp. 15–30.
[25] M. Marcuzzi, M. Buchhold, S. Diehl, and I. Lesanovsky, Phys. Rev. Lett. **116**, 245701 (2016).
[26] M. Buchhold, B. Everest, M. Marcuzzi, I. Lesanovsky, and S. Diehl, Phys. Rev. B **95**, 014308 (2017).
[27] D. Roscher, S. Diehl, and M. Buchhold, Phys. Rev. A **98**, 062117 (2018).
[28] F. Carollo, E. Gillman, H. Weimer, and I. Lesanovsky, Phys. Rev. Lett. **123**, 100604 (2019).
[29] E. Gillman, F. Carollo, and I. Lesanovsky, New J. Phys. **21**, 093064 (2019).
[30] M. Jo, J. Lee, K. Choi, and B. Kahng, Phys. Rev. Research **3**, 013238 (2021).
[31] S. Wolfram, Rev. Mod. Phys. **55**, 601 (1983).
[32] S. Wolfram, *A New Kind of Science* (Wolfram Media, 2002).
[33] see Supplemental Material for details.
[34] M. Jo, J. Um, and B. Kahng, Phys. Rev. E **99**, 032131 (2019).
[35] M. Jo and B. Kahng, Phys. Rev. E **101**, 022121 (2020).
[36] R. Nigmatullin, E. Wagner, and G. K. Brennen, Phys. Rev. Research **3**, 043167 (2021).

Supplemental Material

MEAN-FIELD EQUATIONS FOR THE $(1+1)D$ QCA IN THE MAIN TEXT

In this section we give details on our mean-field analysis for the QCA model discussed in the main text. We directly present results for the asynchronous gate, since the synchronous discrete-time evolution can be obtained by setting the asynchronicity parameter to zero.

In our mean-field analysis, we assume that the reduced state of single rows of the lattice is a product state at any time. This amounts to neglecting correlations within single rows. We furthermore assume that this reduced state is homogeneous, i.e. local single-site properties are equal for all sites belonging to a same row. Because of this assumption, we can drop the index k in the notation of this section. In particular, single-site properties of the reduced state of the QCA at time t are described by the density matrix

$$\rho_t = \begin{pmatrix} \langle n \rangle_t & \frac{x_t - i y_t}{2} \\ \frac{x_t + i y_t}{2} & \langle \bar{n} \rangle_t \end{pmatrix} ,$$

where $x_t = \langle \sigma_x \rangle_t$ and $y_t = \langle \sigma_y \rangle_t$.

The task is then to find a discrete-time equation for updating such a single-site density matrix. Here, we define the update by considering how a single gate application modifies the target site. Due to our assumptions, control sites are in a product state with same single-site density matrix, while the target site before the update is in the empty state. We thus write the state of the three control sites and of the target one, before the update, as

$$\tilde{\rho}_t = \rho_t \otimes \rho_t \otimes \rho_t \otimes \bar{n}. \tag{S1}$$

For later convenience, in the above expression the first two entries of the tensor product represent the two controls on the side of the target site, while the third entry represents the central control which is exactly above the target site [see also Fig. 1(a) in the main text]. The last entry, here consisting of a projector on the empty state, is instead the state of the target site. Exploiting the state $\tilde{\rho}_t$ and considering a single gate application, we can define, within our mean-field analysis, the single-site state of the row at time $t+1$ as

$$\rho_{t+1} = \mathrm{Tr}_{123} \left(G \tilde{\rho}_t G^\dagger \right) . \tag{S2}$$

In the above equation, Tr_{123} denotes the trace over the first three entries of the tensor product in Eq. (S1). The gate G is the four-body gate implementing the local update rules considered in the main text. Here, we rewrite it as

$$G = \Pi \otimes A + \bar{\Pi} \otimes D \, , \qquad \text{where} \qquad D = \sqrt{1-\lambda} B + \sqrt{\lambda} C$$

and

$$A = n \otimes U_{\circ \bullet \circ} + \bar{n} \otimes \mathbb{1} \, , \qquad B = n \otimes U_{\bullet} + \bar{n} \otimes U_{\circ} \, , \qquad C = \sigma_+ \otimes U_{\bullet} U_+ - \sigma_- \otimes U_{\circ} U_+^\dagger \, . \tag{S3}$$

The unitary operators appearing in the above equations are the same reported in the main text. Moreover, we recall here that, in the notation of this section, $\Pi = \bar{n} \otimes \bar{n}$ acts only on the external control sites, and $\bar{n} = |\circ\rangle\langle\circ|$. The other projector is instead $\bar{\Pi} = \mathbb{1} \otimes \mathbb{1} - \Pi$ and also acts solely on the above mentioned control sites.

With the form of the gate and of the state $\tilde{\rho}_t$, we can proceed to evaluate the trace operation in Eq. (S2). We do this in two steps. First, we take the trace with respect to the external control sites, which are described by the first two entries of the tensor products. Defining $\rho_t^{12} = \rho_t \otimes \rho_t$ and $\rho_t^{34} = \rho_t \otimes \bar{n}$, so that $\tilde{\rho}_t = \rho^{12} \otimes \rho^{34}$, we find

$$\mathrm{Tr}_{12} \left(G \tilde{\rho}_t G^\dagger \right) = \langle \Pi \rangle_t^{12} A \rho_t^{34} A^\dagger + \langle \bar{\Pi} \rangle_t^{12} D \rho_t^{34} D^\dagger \, , \tag{S4}$$

where $\langle \cdot \rangle^{12}$ denotes expectation value with respect to the state ρ^{12}.

Then, we can take the trace with respect to the central control site, which was represented by the third entry of the tensor product in Eq. (S1). We do this considering the two different terms of the above equation separately. We start with

$$\mathrm{Tr}_3 \left(A \rho_t^{34} A^\dagger \right) = \langle n \rangle_t^3 U_{\circ \bullet \circ} \bar{n} U_{\circ \bullet \circ}^\dagger + \langle \bar{n} \rangle_t^3 \bar{n} \, ,$$

where $\langle\cdot\rangle_t^3$ denotes expectation value with respect to the state of the central control site, which is — as for the other control sites — ρ_t. The second term on the right-hand-side of Eq. (S4) is slightly more involved since D is made of two terms. Indeed, we have

$$\mathrm{Tr}_3\left(D\rho_t^{34}D^\dagger\right) = (1-\lambda)\,\mathrm{Tr}_3\left(B\rho_t^{34}B^\dagger\right) + \lambda\,\mathrm{Tr}_3\left(C\rho_t^{34}C^\dagger\right) + \sqrt{\lambda}\sqrt{1-\lambda}\left[\mathrm{Tr}_3\left(B\rho_t^{34}C^\dagger\right) + \mathrm{Tr}_3\left(C\rho_t^{34}B^\dagger\right)\right] .$$

A straightforward calculation gives

$$\mathrm{Tr}_3\left(B\rho_t^{34}B^\dagger\right) = \langle n\rangle_t^3 U_\bullet \bar{n} U_\bullet^\dagger + \langle \bar{n}\rangle_t^3 U_\circ \bar{n} U_\circ^\dagger ,$$

$$\mathrm{Tr}_3\left(C\rho_t^{34}C^\dagger\right) = \langle n\rangle_t^3 U_\circ U_+^\dagger \bar{n} U_+ U_\circ^\dagger + \langle \bar{n}\rangle_t^3 U_\bullet U_+ \bar{n} U_+^\dagger U_\bullet^\dagger ,$$

$$\mathrm{Tr}_3\left(B\rho_t^{34}C^\dagger\right) = \langle \sigma_-\rangle_t^3 U_\bullet \bar{n} U_+^\dagger U_\bullet^\dagger - \langle \sigma_+\rangle_t^3 U_\circ \bar{n} U_+ U_\circ^\dagger$$

as well as $\mathrm{Tr}_3\left(C\rho_t^{34}B^\dagger\right) = \mathrm{Tr}_3\left(B\rho_t^{34}C^\dagger\right)^\dagger$. Putting everything together, we arrive at

$$\begin{aligned}
\rho_{t+1} =& \langle\Pi\rangle_t \left(\langle n\rangle_t U_{\circ\bullet\circ} \bar{n} U_{\circ\bullet\circ}^\dagger + \langle\bar{n}\rangle_t \bar{n}\right) + \\
&+ (1-\lambda)\langle\Pi\rangle_t \left(\langle n\rangle_t U_\bullet \bar{n} U_\bullet^\dagger + \langle\bar{n}\rangle_t U_\circ \bar{n} U_\circ^\dagger\right) + \\
&+ \lambda\langle\Pi\rangle_t \left(\langle n\rangle_t U_\circ U_+^\dagger \bar{n} U_+ U_\circ^\dagger + \langle\bar{n}\rangle_t U_\bullet U_+ \bar{n} U_+^\dagger U_\bullet^\dagger\right) + \\
&+ \sqrt{\lambda}\sqrt{1-\lambda}\langle\Pi\rangle_t \left(\langle\sigma_-\rangle_t U_\bullet \bar{n} U_+^\dagger U_\bullet^\dagger - \langle\sigma_+\rangle_t U_\circ \bar{n} U_+ U_\circ^\dagger + \mathrm{h.c.}\right) .
\end{aligned} \tag{S5}$$

This iterative equation allows one to study the dynamics of the QCA as well as its stationary state properties within a mean-field investigation. For instance, to obtain the stationary phase diagram of our QCA reported in the main text, we have numerically simulated the above equation over a sufficiently large number of discrete time-steps.

Additionally, with this expression, we can also compute iterative equations for the dynamics of expectation values. For instance, for the projector n we find

$$\begin{aligned}
\langle n\rangle_{t+1} = \mathrm{Tr}\left(\rho_{t+1} n\right) =& \langle\Pi\rangle_t \langle n\rangle_t q_{\circ\bullet\circ} + \langle\bar{\Pi}\rangle_t \langle n\rangle_t \left[(1-\lambda)p_\bullet + \lambda\left(\sqrt{p_\circ}\sqrt{q} + \sqrt{p}\sqrt{q_\circ}\right)^2\right] + \\
&+ \langle\bar{\Pi}\rangle_t \langle\bar{n}\rangle_t \left[(1-\lambda)p_\circ + \lambda(\sqrt{p_\bullet}\sqrt{q} - \sqrt{p}\sqrt{q_\bullet})^2\right] + \\
&+ \sqrt{\lambda}\sqrt{1-\lambda}\langle\bar{\Pi}\rangle_t \langle\sigma^y\rangle_t \left[\sqrt{q}\,(p_\bullet + p_\circ) + \sqrt{p}\,(\sqrt{p_\circ}\sqrt{q_\circ} - \sqrt{p_\bullet}\sqrt{q_\bullet})\right] .
\end{aligned} \tag{S6}$$

The coefficients in the above equation are reported in the main text. We also note that for the synchronous case $\lambda = 0$, one recovers the equation

$$\langle n\rangle_{t+1} = \langle\Pi\rangle_t \langle n\rangle_t q_{\circ\bullet\circ} + \langle\bar{\Pi}\rangle_t \langle n\rangle_t p_\bullet + \langle\bar{\Pi}\rangle_t \langle\bar{n}\rangle_t p_\circ , \tag{S7}$$

which is also reported in the main text.

MEAN-FIELD EQUATIONS FOR CONTINUOUS-TIME QUANTUM AND CLASSICAL CONTACT PROCESS

In this section, we briefly introduce a quantum contact process model, which, as discussed in the main text, is connected to the physics displayed by our $(1+1)$D QCA.

The quantum contact process that we consider here consists of a one-dimensional spin-1/2 system which undergoes a continuous-time Markovian dynamics. In particular, the dynamics of any operator X of the system obeys the so-called Heisenberg equation [25]

$$\begin{aligned}
\dot{X}_t =& i[H, X_t] + \gamma \sum_k \left(\sigma_k^+ X_t \sigma_k^- - \frac{1}{2}\left\{n_k, X_t\right\}\right) + \kappa_\mathrm{c} \sum_k \left(\bar{\Pi}_k \sigma_k^+ X_t \sigma_k^- \bar{\Pi}_k - \frac{1}{2}\left\{n_k \bar{\Pi}_k, X_t\right\}\right) + \\
&+ \kappa_\mathrm{b} \sum_k \left(\bar{\Pi}_k \sigma_k^- X_t \sigma_k^+ \bar{\Pi}_k - \frac{1}{2}\left\{\bar{n}_k \bar{\Pi}_k, X_t\right\}\right) .
\end{aligned} \tag{S8}$$

In the above equation, the first term accounts for the coherent dynamical contribution associated with the system Hamiltonian. On the other hand, the remaining terms describe incoherent probabilistic processes, which are in fact exactly those of the (classical) contact process. Indeed, the term proportional to γ implements the decay process $\bullet \rightsquigarrow \circ$, the term proportional to $\kappa_{\rm c}$ is instead the coagulation process ($\bullet\bullet \rightsquigarrow \bullet\circ$), while the one proportional to $\kappa_{\rm b}$ is the branching process ($\circ\bullet \rightsquigarrow \bullet\bullet$). Note that, due to the presence of the projector $\bar{\Pi}_k$ these two latter processes can occur at site k only if at least an occupation is present in the neighboring sites of k.

The Hamiltonian of the quantum contact process is the following

$$H = \Omega \sum_k \bar{\Pi}_k \sigma_k^x \ .$$

This Hamiltonian implements both a branching and a coagulation process at the same coherent rate, Ω, via constrained Rabi oscillations at site k that can only occur if the neighbors of k are not simultaneously in the empty state.

We now want to obtain mean-field dynamical equations of motion for the above system. To this end, we consider single-site operators, compute their time derivative according to the action of the generator in Eq. (S11), and make the assumption of uncorrelated state for the system. Following closely the calculations reported in Ref. [26], the mean-field equations of motion for the number operator n (also assuming a homogeneous state) for the quantum contact process is given by

$$\partial_t \langle n \rangle_t = -\gamma \langle n \rangle_t + \Omega \langle \bar{\Pi} \rangle_t \langle \sigma^y \rangle_t + \langle \bar{\Pi} \rangle_t \left[\kappa_{\rm b} - (\kappa_{\rm b} + \kappa_{\rm c}) \langle n \rangle_t \right] \ . \tag{S9}$$

We note that the projector used in our model here is slightly different from the one considered Ref. [26], where $\bar{\Pi}_k = n_{k-1} + n_{k+1}$. This minor difference is not expected to modify the nonequilibrium behavior of the model.

Discretising the above differential equation, and using that $\mathbb{1} = \Pi + \bar{\Pi}$ and $\mathbb{1} = n + \overline{n}$, we find the equation

$$\langle n \rangle_{t+1} = (1 - \gamma \Delta t) \langle \Pi \rangle_t \langle n \rangle_t + (1 - \gamma \Delta t - \kappa_{\rm c} \Delta t) \langle \bar{\Pi} \rangle_t \langle n \rangle_t + \kappa_{\rm b} \Delta t \langle \bar{\Pi} \rangle_t \langle \bar{n} \rangle_t + \Omega \Delta t \langle \bar{\Pi} \rangle_t \langle \sigma^y \rangle_t \ . \tag{S10}$$

We note that by taking $\Omega \Delta t \to 0$ in Eq. (S12) and in Eq. (S13), one recovers the mean-field equations for the classical contact process in continuous-time and in a discrete-time approximation, respectively. In particular, we note that the discrete-time approximation of the dynamical equation of the classical contact process reads

$$\langle n \rangle_{t+1} = (1 - \gamma \Delta t) \langle \Pi \rangle_t \langle n \rangle_t + (1 - \gamma \Delta t - \kappa_{\rm c} \Delta t) \langle \bar{\Pi} \rangle_t \langle n \rangle_t + \kappa_{\rm b} \Delta t \langle \bar{\Pi} \rangle_t \langle \bar{n} \rangle_t \ .$$

Comparing this equation with Eq. (3) in the main text, we find how the rates of the continuous-time contact process can be obtained from the probabilities of our synchronous gate. We indeed find the coagulation rate $\kappa_{\rm c} = (q_{\circ\bullet\circ} - p_\bullet)/\Delta t$, the branching rate $\kappa_{\rm b} = p_\circ / \Delta t$ and decay rate $\gamma = p_{\circ\bullet\circ}/\Delta t$.

MEAN-FIELD EQUATIONS FOR CONTINUOUS-TIME QUANTUM AND CLASSICAL CONTACT PROCESS

In this section, we briefly introduce a quantum contact process model, which, as discussed in the main text, is connected to the physics displayed by our $(1+1)$D QCA.

The quantum contact process that we consider here consists of a one-dimensional spin-1/2 system which undergoes a continuous-time Markovian dynamics. In particular, the dynamics of any operator X of the system obeys the so-called Heisenberg equation [25]

$$\begin{aligned} \dot{X}_t =& i[H, X_t] + \gamma \sum_k \left(\sigma_k^+ X_t \sigma_k^- - \frac{1}{2} \left\{ n_k, X_t \right\} \right) + \kappa_{\rm c} \sum_k \left(\bar{\Pi}_k \sigma_k^+ X_t \sigma_k^- \bar{\Pi}_k - \frac{1}{2} \left\{ n_k \bar{\Pi}_k, X_t \right\} \right) + \\ &+ \kappa_{\rm b} \sum_k \left(\bar{\Pi}_k \sigma_k^- X_t \sigma_k^+ \bar{\Pi}_k - \frac{1}{2} \left\{ \bar{n}_k \bar{\Pi}_k, X_t \right\} \right) \ . \end{aligned} \tag{S11}$$

In the above equation, the first term accounts for the coherent dynamical contribution associated with the system Hamiltonian. On the other hand, the remaining terms describe incoherent probabilistic processes, which are in fact exactly those of the (classical) contact process. Indeed, the term proportional to γ implements the decay process $\bullet \rightsquigarrow \circ$, the term proportional to $\kappa_{\rm c}$ is instead the coagulation process ($\bullet\bullet \rightsquigarrow \bullet\circ$), while the one proportional to $\kappa_{\rm b}$ is the branching process ($\circ\bullet \rightsquigarrow \bullet\bullet$). Note that, due to the presence of the projector $\bar{\Pi}_k$ these two latter processes can occur at site k only if at least an occupation is present in the neighboring sites of k.

The Hamiltonian of the quantum contact process is the following

$$H = \Omega \sum_k \bar{\Pi}_k \sigma_k^x \ .$$

This Hamiltonian implements both a branching and a coagulation process at the same coherent rate, Ω, via constrained Rabi oscillations at site k that can only occur if the neighbors of k are not simultaneously in the empty state.

We now want to obtain mean-field dynamical equations of motion for the above system. To this end, we consider single-site operators, compute their time derivative according to the action of the generator in Eq. (S11), and make the assumption of uncorrelated state for the system. Following closely the calculations reported in Ref. [26], the mean-field equations of motion for the number operator n (also assuming a homogeneous state) for the quantum contact process is given by

$$\partial_t \langle n \rangle_t = -\gamma \langle n \rangle_t + \Omega \langle \bar{\Pi} \rangle_t \langle \sigma^y \rangle_t + \langle \bar{\Pi} \rangle_t \left[\kappa_\mathrm{b} - (\kappa_\mathrm{b} + \kappa_\mathrm{c}) \langle n \rangle_t \right] \ . \tag{S12}$$

We note that the projector used in our model here is slightly different from the one considered Ref. [26], where $\bar{\Pi}_k = n_{k-1} + n_{k+1}$. This minor difference is not expected to modify the nonequilibrium behavior of the model.

Discretising the above differential equation, and using that $\mathbb{1} = \Pi + \bar{\Pi}$ and $\mathbb{1} = n + \overline{n}$, we find the equation

$$\langle n \rangle_{t+1} = (1 - \gamma \Delta t) \langle \Pi \rangle_t \langle n \rangle_t + (1 - \gamma \Delta t - \kappa_\mathrm{c} \Delta t) \langle \bar{\Pi} \rangle_t \langle n \rangle_t + \kappa_\mathrm{b} \Delta t \langle \bar{\Pi} \rangle_t \langle \bar{n} \rangle_t + \Omega \Delta t \langle \bar{\Pi} \rangle_t \langle \sigma^y \rangle_t \ . \tag{S13}$$

We note that by taking $\Omega \Delta t \to 0$ in Eq. (S12) and in Eq. (S13), one recovers the mean-field equations for the classical contact process in continuous-time and in a discrete-time approximation, respectively. In particular, we note that the discrete-time approximation of the dynamical equation of the classical contact process reads

$$\langle n \rangle_{t+1} = (1 - \gamma \Delta t) \langle \Pi \rangle_t \langle n \rangle_t + (1 - \gamma \Delta t - \kappa_\mathrm{c} \Delta t) \langle \bar{\Pi} \rangle_t \langle n \rangle_t + \kappa_\mathrm{b} \Delta t \langle \bar{\Pi} \rangle_t \langle \bar{n} \rangle_t \ .$$

Comparing this equation with Eq. (3) in the main text, we find how the rates of the continuous-time contact process can be obtained from the probabilities of our synchronous gate. We indeed find the coagulation rate $\kappa_\mathrm{c} = (q_{\circ\bullet\circ} - p_\bullet)/\Delta t$, the branching rate $\kappa_\mathrm{b} = p_\circ / \Delta t$ and decay rate $\gamma = p_{\circ\bullet\circ}/\Delta t$.

ESTIMATION OF CRITICAL EXPONENTS

In this section, we provide a brief discussion about the estimation of the critical exponent associated with the decay of the average density of occupied sites, in the example QCA model given by Eq. (6) in the main text. To illustrate this, we consider two horizontal cuts along the phase diagram shown in Fig. 2(b) of the main text. The first, shown in Fig. S1(a), is for $\lambda = 0.55$ while the second, shown in Fig. S1(b), is for $\lambda = 0.90$, thus representing relatively weak/strong asynchronism respectively. As in the paper, the simulations were performed with tensor-network methods, for a bond-dimension of $\chi = 64$, up to time $T = 100$, and two lattice sizes, $L = 128$ and $L = 256$, to demonstrate the finite-size effects in this case.

From the resulting density, $n(t)$, averaged over the entire spatial slice, one can calculate the effective exponent for the power-law decay at criticality as $\alpha(t) = -\log_2(n(t)/n(t/2))$. This will be a constant when the corresponding curve $n(t)$ displays a power-law, allowing for the estimation of the critical exponent for the decay of the average density. Away from the critical line, density curves will then either display an exponentially decaying behaviour towards the absorbing state, or a tendency towards a fixed density. These two behaviours characterise the two phases of the model. In the effective exponent plots, the exponential decay of the density reveals itself as a diverging effective exponent, while the tendency to a fixed density manifests as an effective exponent that tends to zero.

We now consider the first plot of the effective exponent, Fig. S1(a), for $\lambda = 0.55$. In this figure, $L = 128$ is shown as dashed lines, while $L = 256$ is shown as solid lines. The effective exponent for $p_{\bar{n}} = 0.45$ displays behaviour consistent with the absorbing state, while $p_{\bar{n}} = 0.55, 0.6, 0.65$ display behaviour consistent with a tendency to a fixed average density. Finally, the effective exponent for $p_{\bar{n}} = 0.5$ appears to be approaching a value close to 0.16, represented by the dashed horizontal line. The latter is the critical exponent of 1D directed percolation [1]. While this seems clear in this case, note that finite size effects systematically push the density into the absorbing state. In fact, for any finite-size system, eventually all states will fall into the absorbing state. This makes interpretation of such figures, and estimation of critical exponents challenging.

Turning now to Fig. S1(b), for the case of strong asynchronism $\lambda = 0.9$, one can see some of these issues, along with others unique to the model in hand. Here, once again we can see that the curves for $p_{\bar{n}} = 0.7, 0.75$ and 0.8 display a

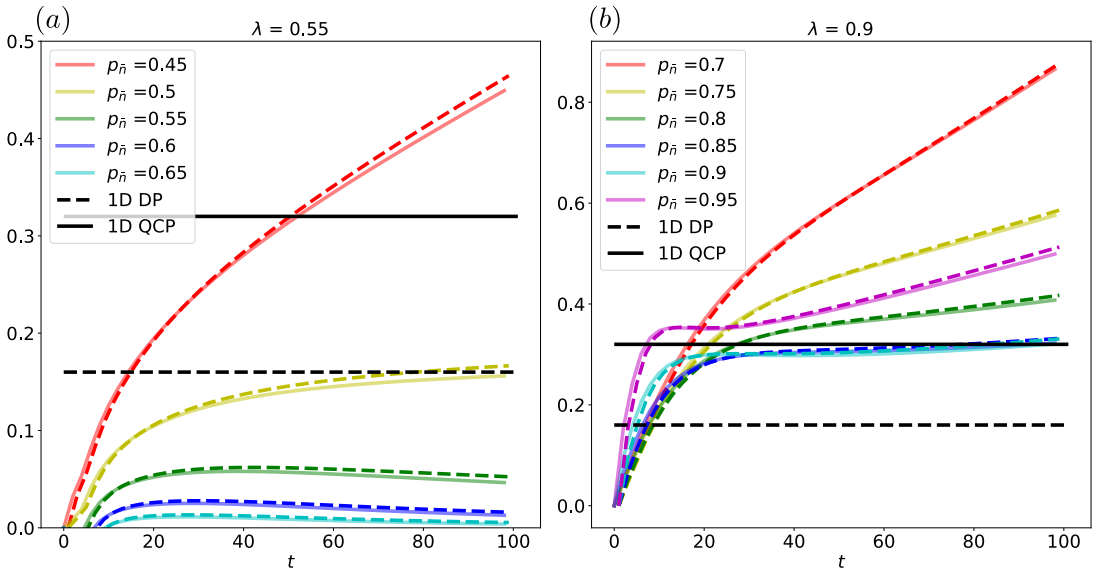

FIG. S1. **Effective Exponents: (a)** Effective exponents for $\lambda = 0.55$. Solid lines are from curves $n(t)$ calculated using $L = 256$, while dashed lines use $L = 128$, see the text for more details. In this plot, the curves can be separated easily into subcritical (tending to an exponential decay and therefore diverging here), critical (a power-law decay, tending to a constant here) and super-critical (tending to a constant and therefore vanishing here). The curves closest to constant appear to tend to a value close to 0.16, which is the critical exponent from the 1D directed percolation universality class. **(b)** Effective exponents for $\lambda = 0.9$. Here, the relatively small region of super-critical states means that all curves appear either sub-critical or close to critical. Taking the the two curves closest to constant, $p_{\bar{n}} = 0.85, 0.9$, one would estimate a critical exponent close to 0.32 (solid horizontal line), which is the estimated value for the critical exponent of the QCP. However, the systematic errors occurring due to finite-size effects make such a conclusion premature, see the text for details.

clear absorbing state behaviour similar to that of Fig. S1(a). Following that, the curves $p_{\bar{n}} = 0.85, 0.9$ appear rather flat on this scale, indicating approximate power-laws. However, following around $T = 50$, they start to lift again into the absorbing state. Precisely due to the systematic nature of the finite-size errors, it is hard to say whether these are genuinely critical curves subject to finite-size errors, or simple absorbing state curves with longer relaxation time-scales than other curves in the plot. This is exemplified by the final curve $p_{\bar{n}} = 0.95$: initially this curve appears rather flat, up to around $T = 30$. However, following this it shows behaviour consistent with an exponential decay. We note that this behaviour is rather different from that displayed by the curves for $\lambda = 0.55$, which show no such initial flattening. Furthermore, we note that while one might naively expect $p_{\bar{n}} = 0.95$ to be a fixed density state [similar to how increasing $p_{\bar{n}}$ in Fig. S1(a) led from sub-critical to critical to super-critical] in fact it is absorbing. This is consistent with the increasingly thin region of super-critical states with lambda, as can be seen in Fig. 2 of the main text. Studying the high asynchronism region effectively would thus require a much finer grid, which in turn would require much longer simulation times to allow the curves to be distinguished (thus also requiring much larger system sizes to avoid finite-size effects).

Finally, we note that, in the case that the curves with $p_{\bar{n}} = 0.85, 0.9$ are used to estimate the critical exponent for $\lambda = 0.9$, the estimated value lies close to 0.32, represented by the solid horizontal line. This is the value estimated for the continuous-time quantum contact process [28, 30]. While it is tempting to conclude based on this that there is indeed a change of universal behaviour in the non-perturbative phase diagram, such a claim requires more extensive simulations, including both much larger lattice sizes, longer simulation times and finer parameter grids.